Refinement of Near Earth Asteroids' orbital elements via simultaneous measurements by two observers

Siegfried Eggl

Noname manuscript No.
(will be inserted by the editor)

Refinement of Near Earth Asteroids' Orbital Elements via Simultaneous Measurements by Two Observers

S. Eggl

Received: date / Accepted: date

Abstract The aspects of triangulation of Near Earth Asteroids by two arbitrarily positioned observers (space- and earth-bound) are being investigated, and the resulting orbital elements are compared to those gained through common orbital determination and refinement techniques. The main advantages of the method proposed in this work are, that given the approximate position of an asteroid, high quality orbital elements can be acquired very rapidly using two observations only.

Keywords orbit determination · orbit refinement · near earth asteroids · orbital elements · triangulation · very short arc observations

1 Introduction

Since the collision of comet Shoemaker-Levy 9 with Jupiter in 1994, which demonstrated implications of impacts of Solar System's small bodies on planets very illustratively, threat assessment concerning Near Earth Objects has become a greater public demand. Therefore knowledge of the actual number of asteroids in the vicinity of Earth, as well as data on their orbits are required. Current observation programs concerning Near Earth Asteroids (NEAs) are aiming at compiling a complete catalog of kilometer-sized objects. Their focus mostly lies on the identification of unknown objects and calculation of preliminary orbital elements being the basis of follow up observations, that allow for plausible predictions on impact hazards. As identification runs often tend to produce so-called Very Short Arc (VSA) observations, meaning that data on the object's trajectory is available for a very short period of time only, usual orbit determination techniques such as Gaussian or Laplacian hardly produce reliable predictions on future positions, which are essential for follow up observations. Milani et al. (2004) developed methods using data of VSA observations to confine the possible parameter-space of NEAs locations and movements. They are able to define a so-called "admissible region" restricting the space of an asteroid's viable ephemerides for a certain period of time. Their predictions could be proven to be valid for some weeks at

S. Eggl
Institute for Astronomy, University of Vienna, Türkenschanzstr. 17, A-1180 Wien, Austria

least, still it is not yet possible to do a full orbit determination for Solar System objects with this method, even though a possible strategy for Earth-bound space debris has been proposed (Tommei et al., 2007). Ideally more VSA observations of the same object can be combined to gain access to orbital elements - the so-called "linkage problem" (Milani & Gronchi, 2009) - using "attributables" (Milani et al., 2001), i.e. angular positions and velocities of the body on the celestial sphere at given epochs (see e.g. Gronchi et al. (2010)).

The fact, that follow up programs cannot always be performed soon after an initial detection, leads to situations where already identified objects are mistaken for others or even "lost" again. Apart from these problems concerning refinements of initial orbits, Near Earth Asteroids are subject to very complex gravitational interactions with the planets, causing a permanent change in asteroids' orbital elements (Morbidelli et al., 2003). This makes precise measurements and frequent updates of orbital elements absolutely necessary.

By using simultaneous measurements of two independent observing facilities, the triangulation method proposed in this paper is capable of producing highly accurate orbital elements with a minimum of observations necessary, once the approximate position of the asteroid is known. Being preferably space-based and allowing for fast and precise determination of orbital elements, this method would be predestined for quick follow ups as well as frequent updating measurements, ensuring that discovered objects stay within eye-spot.

2 Previous Work and Current Accomplishments

The current success of spaceborne missions in detecting NEAs, e.g. WISE (Wright et al., 2010), suggests a greater emphasis on such endeavours in the future. Yet, the basic idea of using two simultaneous observations from spacecraft to improve orbital elements was brought up by R. Dvorak in 2003 [1] and has been consequently investigated by Gromaczkiewicz (2006). The configuration then proposed can be seen in Figure 1. With $\mathbf{S}_1$ and $\mathbf{S}_2$ being the known position-vectors of two observation-points in the Solar-System, the goal is to determine the orbital elements of a celestial body having a heliocentric position-vector $\mathbf{H}$. Following a purely trigonometric Ansatz, Gromaczkiewicz (2006) showed, that the position-vector $\mathbf{H}$ can be obtained from a simultaneous measurement of two pairs of angles in $\mathbf{S}_1$ and $\mathbf{S}_2$, if the distance between these two points $\|\mathbf{S}_1\mathbf{S}_2\|$ is known. Taking two of those measurements at different times, a velocity vector can be linearly interpolated and orbital elements calculated. His method, however, was proven to be confined to spacecraft configurations within the ecliptic (Eggl, 2008) as well as to be prone to computational round-off errors due to a frequent occurrence of trigonometric functions with non-constant arguments in denominators.

In this work, nearly all trigonometric elements have been replaced by transformations to affine coordinate systems, eliminating most denominators containing trigonometric functions, that may have given rise to singularities at certain observer-asteroid configurations. The remaining "unfavorable configurations" (UC) are identified via error propagation formulae. The change from a purely trigonometric treatment to a synthesis of trigonometric and algebraic manipulations also solved the problem of the observers'

[1] Dvorak, R.: private communication, University of Vienna, (2003)

confinement to the ecliptic plane, meaning that the spacecraft may be placed completely arbitrarily now. In order to check the quality of the orbital elements produced by the new method, simulations of observations as well as measurements of fictitious and real NEAs have been performed and compared to orbital data published by the Solar System Dynamics Group, JPL (2010).

The further outline of this paper will be as follows: section 3 contains a short walk-through of the triangulation method, including an error propagation analysis. In sections 4 and 5, the results of the simulated orbit-refinement are presented, and will be discussed in section 6.

3 Theoretical Description of the Proposed Orbit Refinement Method

This section contains a walk-through of the triangulation method, describing step by step how orbital elements of the observed celestial body can be obtained from simultaneous angular measurements from two spacecraft with known positions, as well as a theoretical analysis of its error propagation behavior.

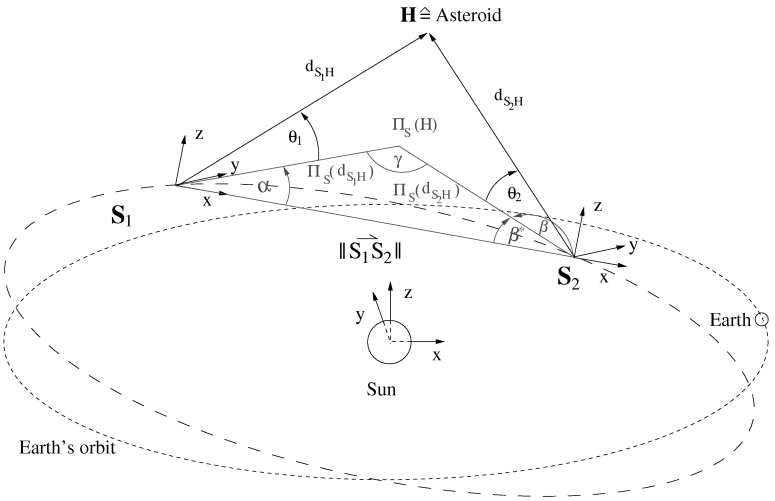

Fig. 1 A view on the ecliptic; the Earth's orbit (dotted), as well as the orbit of the observing spacecraft (dashed) are to be seen in a heliocentric coordinate system. $\mathbf{S}_1$ and $\mathbf{S}_2$ denote the positions of the spacecraft, $\mathbf{H}$ the observed celestial body. α and β, are the angles to be measured in an arbitrary plane S, containing $\mathbf{S}_1$ as well as $\mathbf{S}_2$ and θ_1 and θ_2 are angles onto S, to be measured at $\mathbf{S}_1$ and $\mathbf{S}_2$ respectively. Note, that in the configuration following Gromaczkiewicz (2006) β is measured counterclockwise, starting at the connection line between $\mathbf{S}_1$ and $\mathbf{S}_2$. This will correspond to the angle β^* in the reformulated version of Eggl (2008). $\mathbf{S}_1$ and $\mathbf{S}_2$ do not necessarily have to share the same orbit.

3.1 Orbit Determination via Triangulation

For the localization of a celestial body $\mathbf{H}$ and a consequent orbit determination, the following data are required (see Figure 1):

– the heliocentric position-vectors of the observing spacecraft $\mathbf{S}_1$ and $\mathbf{S}_2$
– an arbitrary reference plane S containing $\mathbf{S}_1$ as well as $\mathbf{S}_2$
– angles in $\mathbf{S}_1$: α, θ_1
– angles in $\mathbf{S}_2$: β, θ_2

The next steps are as follows:

1. Given $\mathbf{S}_1$ and $\mathbf{S}_2$ the distance $d_{S_1S_2}$ can be calculated.

$$d_{S_1S_2} = \|\mathbf{S}_2 - \mathbf{S}_1\|$$

2. Angles α and β are transformed into α^* and β^* denoting angles in the triangle $\mathbf{S}_1\mathbf{S}_2\Pi_S(\mathbf{H})$ in the plane S, where $\Pi_S(\mathbf{H})$ denotes the orthogonal projection of $\mathbf{H}$ onto S (see Figure 1).

$$\begin{aligned} &\alpha^* = \alpha,\ \beta^* = \pi - \beta && \text{for } \alpha, \beta \leq \pi \\ &\alpha^* = 2\pi - \alpha,\ \beta^* = \beta - \pi && \text{for } \alpha, \beta > \pi \\ &\gamma = \pi - \alpha^* - \beta^* \end{aligned}$$

γ, the third angle in the triangle $\mathbf{S}_1\mathbf{S}_2\Pi_S(\mathbf{H})$ can be acquired through the triangle's angular sum.

3. Using trigonometric relations, one calculates the distances $\Pi_S(d_{S_1H})$ and $\Pi_S(d_{S_2H})$ (see Figure 1).

$$\Pi_S(d_{S_1H}) = d_{S_1S_2} \cdot \frac{sin(\beta^*)}{sin(\gamma)} \qquad \Pi_S(d_{S_2H}) = d_{S_1S_2} \cdot \frac{sin(\alpha^*)}{sin(\gamma)} \tag{1}$$

4. Dividing by the cosine of the vertical angles θ_1 and θ_2 transforms the projected distances $\Pi_S(d_{S_1H}), \Pi_S(d_{S_2H})$ into the true distances of the observing facilities $\mathbf{S}_1$ and $\mathbf{S}_2$ from the celestial body.

$$d_{S_1H} = \frac{\Pi_S(d_{S_1H})}{cos(\theta_1)} \qquad d_{S_2H} = \frac{\Pi_S(d_{S_2H})}{cos(\theta_2)} \tag{2}$$

5. So, a full set of polar coordinates for the celestial body $\mathbf{H}$ in the affine coordinate systems Sys_1 and Sys_2, centered at the observers' positions, is available.

$$\begin{aligned} &\mathbf{H}_{r_{Sys_1}} = d_{S_1H} && \mathbf{H}_{r_{Sys_2}} = d_{S_2H} \\ &\mathbf{H}_{\phi_{Sys_1}} = \alpha && \mathbf{H}_{\phi_{Sys_2}} = \beta \\ &\mathbf{H}_{\theta_{Sys_1}} = \theta_1 && \mathbf{H}_{\theta_{Sys_2}} = \theta_2 \end{aligned}$$

6. Those polar coordinates can be transferred into Cartesian coordinates denoting the position of $\mathbf{H}$ in the systems Sys_1 and Sys_2.

$$\begin{pmatrix} \mathbf{H}_{r_{Sys_1}} \\ \mathbf{H}_{\phi_{Sys_1}} \\ \mathbf{H}_{\theta_{Sys_1}} \end{pmatrix} \rightarrow \begin{pmatrix} \mathbf{H}_{x_{Sys_1}} \\ \mathbf{H}_{y_{Sys_1}} \\ \mathbf{H}_{z_{Sys_1}} \end{pmatrix} \qquad \begin{pmatrix} \mathbf{H}_{r_{Sys_2}} \\ \mathbf{H}_{\phi_{Sys_2}} \\ \mathbf{H}_{\theta_{Sys_2}} \end{pmatrix} \rightarrow \begin{pmatrix} \mathbf{H}_{x_{Sys_2}} \\ \mathbf{H}_{y_{Sys_2}} \\ \mathbf{H}_{z_{Sys_2}} \end{pmatrix} \tag{3}$$

7. In order to transform the position vectors $\mathbf{H}_{Sys_1}$ and $\mathbf{H}_{Sys_2}$ into heliocentric position vectors, the two coordinate systems Sys_1, and Sys_2 are chosen to have their origins in the points $\mathbf{S}_1$ and $\mathbf{S}_2$ respectively (see Figure 1). Those systems are oriented in such a way, that their first base-vector $\mathbf{b}_1$ denoting the new x-axis aligns with the vector $\mathbf{S}_1\mathbf{S}_2$ connecting the points $\mathbf{S}_1$ and $\mathbf{S}_2$. The second base-vector $\mathbf{b}_2$ can be chosen to be e.g. the position vector $\mathbf{S}_1$.[2] As shown in Figure 1 the second base-vector can be chosen to be in the plane S defined by the points $\mathbf{S}_1$, $\mathbf{S}_2$ and the Sun. Therefore one could take e.g. the position vector $\mathbf{S}_1$ leaving the orthonormalization to the following Gram-Schmidt procedure. As the requirements for the new coordinate systems are somewhat arbitrary, except being equally orientated and having the x-axis aligned with $\mathbf{S}_1\mathbf{S}_2$, another possible way of finding the second base-vector simply consists of an intermittent change to heliocentric polar coordinates, adding 90° $(= \frac{\pi}{2})$ to the horizontal angle ϕ of $\mathbf{b}_1$.[3]
   The third base-vector $\mathbf{b}_3$ can be obtained through the cross product of $\mathbf{b}_1$ and $\mathbf{b}_2$
8. If the base, that has been chosen, is orthogonal, then its vectors $(\mathbf{b}_1, \mathbf{b}_2, \mathbf{b}_3)$ are to be normalized, in order to gain an orthonormal base B consisting of the normalized vectors $\mathbf{b}$ called $(\mathbf{c}_1, \mathbf{c}_2, \mathbf{c}_3)$.
   Alternatively, having gained a non-orthogonal base, one may use the Gram-Schmidt procedure to receive a set of orthonormal base-vectors $(\mathbf{c}_1, \mathbf{c}_2, \mathbf{c}_3)$.
9. Consequently the position of the celestial body $\mathbf{H}$ can be transformed from systems Sys_1 and Sys_2 into the heliocentric system Sys_0.

$$\mathbf{H}_{Sys_0} = B \cdot \mathbf{H}_{Sys_1} + \mathbf{S}_1, \qquad \mathbf{H}_{Sys_0} = B \cdot \mathbf{H}_{Sys_2} + \mathbf{S}_2$$

   At a first glance it seems like there were two different equations for the heliocentric position-vector $\mathbf{H}_{Sys_0}$, that could be used to achieve some error reduction in a statistical way. Unfortunately these equations are not independent, for they are related via the common angle γ that had to be used to calculate radial distances from $\mathbf{H}$ to $\mathbf{S}_1$ and $\mathbf{S}_2$ respectively.
10. If more than one observation has been performed, the data acquired at different times can be used to estimate the velocity-vector of $\mathbf{H}$. The two basic methods to gain velocities are linear interpolation, requiring two positions of $\mathbf{H}$ only, or the Stirling-interpolation using three observations (see e.g. Vesely (2001)).
11. Using position-, and velocity-vectors of $\mathbf{H}$, orbital elements can be calculated (see e.g. Guthmann (2000)).

Figure 1 may suggest, that the observing spacecraft would have to share the same orbit. In fact this is not the case, as the measurement reference plane S does not have to remain constant in time. It can easily be constructed individually for each measurement without influencing positioning results for $\mathbf{H}$. Though, it must be fixed during one measuring process, which is usually being achieved by requiring quick and simultaneous measurements in $\mathbf{S}_1$ and $\mathbf{S}_2$.

[2] Orthogonality is not a must for the choice of the second base-vector, as the real orthonormalization of the whole base will be ensured by the following Gram-Schmidt procedure.

[3] Note, that the later method does not exactly correspond to Figure 1, because $\mathbf{b}_2$ will no more lie in the plane spanned by $\mathbf{S}_1$, $\mathbf{S}_2$ and the Sun.

3.2 Suggested way of measurement

As proposed in this paper, the method will serve as a quick and reliable improvement of orbital elements of asteroids. Therefore it must be assumed, that a preliminary positioning of the asteroid (**H**) has already been performed, in order to fix the orientation of both observing spacecraft to the particular segment of the celestial sphere, containing **H**. Given a positive identification of **H** from both observers, the angular distances of **H** to guiding stars in the respective stellar background observed by $\mathbf{S}_1$ and $\mathbf{S}_2$ are to be measured simultaneously. This data, together with the positions of $\mathbf{S}_1$ and $\mathbf{S}_2$ are sent back to the control station, where α, θ_1 for $\mathbf{S}_1$ and β, θ_2 for $\mathbf{S}_2$ respectively can be evaluated and the exact positioning of **H** may be performed. One further observation conducted after the proper motion of **H** caused a noticeable shift in its measured position will result in a full set of orbital elements. Every further observation can be used to increase the quality of these elements.

3.3 Correlations between observables

From a trigonometric point of view, the measured angles α, β, θ_1 and θ_2 are situated in a tetrahedron spanned by the points $\mathbf{S}_1, \mathbf{S}_2, \mathit{\Pi}_S(\mathbf{H})$ and **H**. Therefore they are correlated via the tetrahedron relation:

$$sin(\alpha)sin(\frac{\pi}{2}-\theta_1)sin(\theta_2) = sin(\beta)sin(\frac{\pi}{2}-\theta_2)sin(\theta_1)$$

which can be simplified to

$$sin(\alpha)tan(\theta_2) = sin(\beta)tan(\theta_1) \tag{4}$$

Relation (4) will not be used to eliminate one of the observables, as this would come at the cost of adding trigonometric functions to denominators within the global method, which in turn causes an increase in singularities. Also, the possible gain in doing so is small, for a second observation site would still be required. It may, however, serve as a valuable tool to check on correct alignment and aiming of the two observing sites.

3.4 Error Propagation Behavior

A large part of the triangulation method developed in (3.1) consists of linear transformations, so the interesting aspects - from the point of error propagation behavior - are equations (2). Being of similar structure, it is sufficient to perform a propagation of absolute errors for one of these equations:

$$d_{S_1H} = \frac{\mathit{\Pi}_S(d_{S_1H})}{cos(\theta_1)} \tag{5}$$

Using equation (1) we get for $\alpha, \beta \leq \pi$:

$$\mathit{\Pi}_S(d_{S_1H}) = d_{S_1S_2} \cdot \frac{sin(\beta^*)}{sin(\gamma)}, \qquad \gamma = \pi - \alpha - \beta^*$$

$$\begin{aligned} d_{S_1H} &= \frac{d_{S_1S_2}}{cos(\theta_1)} \cdot \frac{sin(\beta^*)}{sin(\pi - \alpha - \beta^*)} \\ &= \frac{d_{S_1S_2}}{cos(\theta_1)} \cdot \frac{sin(\beta^*)}{sin(\alpha + \beta^*)} \end{aligned} \tag{6}$$

The absolute error of d_{S_1H}, denoted by Δd_{S_1H}, can be calculated as follows, all Δ being unsigned:

$$\begin{aligned} \Delta d_{S_1H} \leq & |\frac{\partial d_{S_1H}}{\partial \alpha}| \cdot \Delta\alpha + |\frac{\partial d_{S_1H}}{\partial \beta^*}| \cdot \Delta\beta^* + \\ & |\frac{\partial d_{S_1H}}{\partial \theta_1}| \cdot \Delta\theta_1 + \\ & |\frac{\partial d_{S_1H}}{\partial d_{S_1S_2}}| \cdot \Delta d_{S_1S_2} \end{aligned}$$

Evaluating the partial derivatives holds the following expression for Δd_{S_1H}:

$$\begin{aligned} \Delta d_{S_1H} \leq & \; d_{S_1S_2} \cdot (|\frac{sin(\beta^*)}{cos(\theta_1)} \cdot \frac{cot(\alpha+\beta^*)}{sin(\alpha+\beta^*)}| \cdot \Delta\alpha + \\ & |\frac{sin(\alpha)}{sin(\alpha+\beta^*)^2 \cdot cos(\theta_1)}| \cdot \Delta\beta^* + \\ & |\frac{sin(\beta^*)}{sin(\alpha+\beta^*)} \cdot \frac{tan(\theta_1)}{cos(\theta_1)}| \cdot \Delta\theta_1) + \\ & |\frac{sin(\beta^*)}{sin(\alpha+\beta^*) \cdot cos(\theta_1)}| \cdot \Delta d_{S_1S_2} \end{aligned} \tag{7}$$

A similar expression for Δd_{S_2H} may easily be derived by switching the horizontal angles α and β^* and exchange the vertical angle θ_1 with θ_2.

The values of Δd_{S_1H} for different angles α, β^* and θ_1 can be seen in Figure 2, Table 1 shows the exact parameters used. The left picture in Figure 2 shows, that the error in the calculated distance d_{S_1H} grows very fast, if the sum of α and β^* comes close to $\pi = 180^\circ$, or both angles become zero. Those are the cases, when the triangle $\mathbf{S_1HS_2}$ dissolves, because all three points are on the same line. A similar behavior can be observed when looking at the right picture, except that β^* has been fixed to 90°, in order to vary θ_1. When the variable horizontal angle (α or β^*) approaches 90°, there will be no triangle either, because the lines including d_{S_1H} and d_{S_2H} will not intersect in finite space. Measurement errors will have large effects in those regions especially. Taking into account given symmetries in the problem, it is obvious, that fixing α and varying β^* will yield similar results, which has also been found in (Eggl, 2008).

In summary, this error propagation analysis supports the intuitive arguments claiming that the triangulation method will cause problems in *"unfavorable configurations"* - i.e. when the triangle $\mathbf{S_1HS_2}$ collapses. Fortunately, these cases are rare and closely packed in the parameter-space. It has also been shown, that increased measurement errors do not change the method's global behavior (Eggl, 2008).

From the fact, that the measurement triangle will dissolve given too large observational errors on the angular measurements, one can derive a limiting separation of the observation sites (Δ_{min}) as a function of the asteroid's distance to the center of the connecting baseline ($d = \|\mathbf{H} - \frac{\mathbf{S_1S_2}}{2})\|$) and the error in angular measurements e.g. $\Delta\alpha$:

$$\Delta_{min} = 2d \cdot tan(\Delta\alpha) \tag{8}$$

The main assumption hereby was, that the angles α and β^* as well as their errors are being of the same size, so that 'outer' limiting vectors towards $\mathbf{H}$ emerging from the observers at total angles $\alpha + \Delta\alpha$ and $\beta^* + \Delta\beta^*$ become parallel.

Fig. 2	α [°]	β^* [°]	θ_1 [°]	$d_{S_1S_2}$ [AU]	$\Delta\alpha$ ["]	$\Delta\beta^*$ ["]	$\Delta\theta_1$ ["]	Δd_{S_1H} [AU]
l	0 to 180	0 to 180	fixed 45	1	1	1	1	10^{-7}
r	0 to 180	fixed 90	-90 to 90	1	1	1	1	10^{-7}

Table 1 Parameters used for absolute error propagation of equation (2). See Figure 2; l denotes the left picture, r the right one.

4 Simulation of Observations

In order to be able to test the performance of the orbit refinement method presented in section (3.1), some data on measurements have to be acquired. This was done by simulating the observation-process in parallel to the time-propagation of the main Solar System bodies via numerical integration of the non-relativistic equations of motion using the order controlled Lie-Series Integrator (Hanslmeier, Dvorak, 1984), (Eggl, Dvorak, 2010). Target of this virtual observation is to gain position angles for the celestial body **H** as would be measured by the observing spacecraft $\mathbf{S}_1$ and $\mathbf{S}_2$, as well as the respective distance of the spacecraft $\|\mathbf{S}_1\mathbf{S}_2\|$ for all output-times of the numerical integration.

4.1 Optional Error-Sources for the Virtual Measurement

Additionally, four optional error-sources have been included in the simulation of the measurement process for the scenario to become more realistic.

- positioning error of **H** due to random deviations in angle-measurements
- check for measurement-blockades due to occultation of the line of sight between one observer and **H** by the Sun
- positioning error of **H** due to differences in light travel time from **H** to $\mathbf{S}_1$ and $\mathbf{S}_2$
- positioning error of **H** due to deviations of distance measurements between $\mathbf{S}_1$ and $\mathbf{S}_2$

4.1.1 Positioning Error of **H** *due to Random Deviations in Angle Measurements*

Deviations in measurements of the angles α, β, θ_1 and θ_2 are, in general, unavoidable. They are, of course, dependent on the way of angle determination. Some uncertainties are caused by e.g. the finite resolution capacities of the imaging apparatus of the observing spacecraft, meaning that some solid angle mapped inside a pixel draws an uncertainty region for the position of **H** on the corresponding celestial sphere of the observer. This uncertainty region is simulated by randomly adding or subtracting a fixed error ϵ to each angle during every measurement. For the simulations in section 5, ϵ has been chosen corresponding to a 1 $[m]$ diameter, refraction limited, optical (500 $[nm]$), space-based telescope ($\epsilon = 0.125822$ ["]), a similar setting with a diameter of 0.3 $[m]$ ($\epsilon = 0.419405$ ["]), as well as an Earth-based telescope ($\epsilon = 2$ ["]).

4.1.2 Positioning Error of **H** *due to Deviations of Distance Measurements between* $\mathbf{S}_1$ *and* $\mathbf{S}_2$

The simulation of a measurement uncertainty (ΔS) of the distance $\|\mathbf{S}_1\mathbf{S}_2\|$ has been implemented as follows: A unit vector $\frac{\mathbf{R}}{\|\mathbf{R}\|}$ of random direction is being determined,

and stretched to the length representing the required displacement error ΔS. The displacement vector $\mathbf{Z}$ is then added to, or subtracted from the real positions $\mathbf{S}$ of the observers, resulting in new positions $\mathbf{S}^n$. Since the measurement of the angles is performed at the correct position, of the spacecraft, their values remain unaltered.

$$\mathbf{Z} = \Delta S \cdot \frac{\mathbf{R}}{\|\mathbf{R}\|}, \qquad \mathbf{S}^n = \mathbf{S} + \mathbf{Z}$$

4.1.3 Measurement Blockades due to Occultation of the Line Of Sight between One Observer and $\mathbf{H}$ *by the Sun*

In principle, the line of sight between an observing spacecraft and the observed celestial object can be broken by any Solar System's body. In practice, the Sun is the only object in the inner Solar System having an angular diameter that is not to be neglected when observed from a distance of approximately 1 $[AU]$. Therefore the possibility of an occultation has to be taken into account and was included in the simulations performed (see Figure 3).

The one important parameter governing this behavior is the scalar normal-distance of the vector of the line of sight to the Sun, which can be expressed by:

$$\mathbf{a} = \mathbf{S}_1\mathbf{H} = \mathbf{H} - \mathbf{S}_1, \qquad \mathbf{r_0} = \mathbf{S}_1$$
$$d_1 = \| \frac{\mathbf{a}}{\|\mathbf{a}\|} \times (-\mathbf{r}_0) \|$$

d_1 denotes the scalar normal-distances of the line of sight $\mathbf{S}_1\mathbf{H}$ to the center of the coordinate system, which corresponds to the center of the Sun, as we are using heliocentric coordinates. The same procedure can be applied in order to calculate d_2, the line of sight for $\mathbf{S}_2\mathbf{H}$. Of course, a blocking radius of the Sun has to be taken into account ($r_\odot \simeq 696000km \simeq 0.00465247AU$). Assuming flawless baffling, and the Sun's approximately spherical shape, the modified distances d_1', d_2' to the rim of the Sun are:

$$d_1' = d_1 - r_\odot \qquad\qquad d_2' = d_2 - r_\odot$$

If one of the distances $d_1', d_2' < 0$, then the corresponding line of sight will be broken, and an orbit determination will become impossible.

4.1.4 Positioning Error of $\mathbf{H}$ *due to Differences in Light Travel Time from* $\mathbf{H}$ *to* $\mathbf{S}_1$ *and* $\mathbf{S}_2$

The fact that information on the location of the NEAs travels with light speed may cause some measurement errors, as we are dealing with distances in the order of Astronomical Units.[4] Define the light travel time of the information of the asteroid's location $\mathbf{H}$ to the spaceborne observatories $\mathbf{S}_1$ and $\mathbf{S}_2$ as t_1 and t_2. As can be seen in Figure 4 the positioning of NEA $\mathbf{H}$ yields different results depending on the actual information on the location of $\mathbf{H}$ that has arrived at the respective observation site. The differences in positioning results depend on the distances $\|\mathbf{S}_1\mathbf{H}\|, \|\mathbf{S}_2\mathbf{H}\|$ as well as the speed of

[4] The effects of General Relativity are not taken into account here.

the observed celestial body, $\mathbf{v}_H$. In order to simulate this effect, the positions of $\mathbf{H}$ in systems Sys_1 and Sys_2 have to be adapted as follows[5]

$$r_{Sys_1} = \|\mathbf{S}_1\mathbf{H}\|, \qquad r_{Sys_2} = \|\mathbf{S}_2\mathbf{H}\|, \qquad \Delta r = r_{Sys_1} - r_{Sys_2}, \qquad \Delta t = \frac{|\Delta r|}{c}$$

$$\Delta\mathbf{H} = \mathbf{v}_H \cdot \Delta t$$

$$\begin{aligned} \mathbf{H}_{Sys_1} &= \mathbf{H}_{Sys_1} - \Delta\mathbf{H} \quad \text{for} \quad \Delta r > 0 \\ \mathbf{H}_{Sys_2} &= \mathbf{H}_{Sys_2} - \Delta\mathbf{H} \quad \text{for} \quad \Delta r < 0 \end{aligned}$$

In practice, the errors resulting from this effect are very hard to counter, as neither the velocities $\mathbf{v}_H$ nor the distances r_{Sys_1} and r_{Sys_2} are known initially. Still, having first approximations of the location and velocity of $\mathbf{H}$, an estimate on the size of this effect can be obtained, which in turn can be used to calculate new positions and velocities. If such an iterative process does indeed converge, is topic of future investigations.

4.2 Simulation Analysis

For the quantitative evaluation, ΔH and Δv_H curves are being generated, denoting the difference of the triangulated quantities to their "true" values, e.g. difference of position vector $\mathbf{H}$ gained by triangulation to the position vector that is taken directly from the numerical integration.

$$\begin{aligned} \Delta H &= \|\Delta\mathbf{H}\| = \|\mathbf{H}_{integration} - \mathbf{H}_{triangulation}\| \\ \Delta v_H &= \|\Delta\mathbf{v_H}\| = \|\mathbf{v}_{\mathbf{H}_{integration}} - \mathbf{v}_{\mathbf{H}_{triangulation}}\| \end{aligned}$$

As these quantities can be evaluated after every time-step of a numerical integration, statistical evaluation methods may be applied.

$$\begin{aligned} \Delta H_{max} &= sup\{\Delta H\}, \qquad \Delta v_{H_{max}} = sup\{\Delta v_H\} \\ \Delta H_{min} &= inf\{\Delta H\}, \qquad \Delta v_{H_{min}} = inf\{\Delta v_H\} \end{aligned}$$

ΔH_{max} and $\Delta v_{H_{max}}$ denote the maximum values, ΔH_{min} and $\Delta v_{H_{min}}$ the minimum values of the corresponding quantities. As was shown in section 3.4 "unfavorable configurations" may lead to sudden leaps in errors causing statistical "outriders". For this reason, the use of the arithmetic mean as a statistical tool is not recommendable. A method known to me more robust in such cases is the statistical *median*. Introducing the median of quantities ΔH and Δv_H as $\widetilde{\Delta H}$ and $\widetilde{\Delta v}_H$, let us call the corresponding statistical deviation "median-deviation" $(\widetilde{D}_{\Delta H}, \widetilde{D}_{\Delta v_H})$. Those can be defined as follows (Sachs, 1999):

$$\begin{aligned} \widetilde{\Delta H} &= median(\Delta H_i) \quad \text{with } \Delta H_i \in \{\Delta H\},\ i \in \mathbb{N} \\ \widetilde{\Delta v}_H &= median(\Delta v_{H_i}) \quad \text{with } \Delta v_{H_i} \in \{\Delta v_H\},\ i \in \mathbb{N} \end{aligned}$$

$$\begin{aligned} \widetilde{D}_{\Delta H} &= median(|\Delta H_i - \widetilde{\Delta H}|) \quad \text{with } \Delta H_i \in \{\Delta H\},\ i \in \mathbb{N} \\ \widetilde{D}_{\Delta v_H} &= median(|\Delta v_{H_i} - \widetilde{\Delta v}_H|) \quad \text{with } \Delta v_{H_i} \in \{\Delta v_H\},\ i \in \mathbb{N} \end{aligned}$$

[5] c denotes vacuum light speed, in system units: $c \simeq 174.89411491074148\ [\frac{AU}{(ephemeric)D}]$. The adaption of the positions of $\mathbf{H}$ has to be performed before the calculation of measurement angles.

	a [AU]	e []	i [°]	ω[°]	Ω[°]	M[°]	mass[$M_\odot$]
$\mathbf{S}_1$	1.00000261	0.01671123	-0.00001531	102.9376819	0	57.5268897	0
$\mathbf{S}_2$	1.00000261	0.01671123	-0.00001531	102.9376819	0	297.5268897	0
$\mathbf{H}$	2	0.5	30	0	0	0	0

Table 2 Initial orbital elements for epoch J2000 of observers S_1, S_2 and the asteroid **H**

4.3 Simulation of Orbit Determination of Fictitious Asteroids

In order to get a feeling for the behavior of the simulated orbit refinement method, test-calculations with fictitious NEAs have been performed (Eggl, 2008), including circular, elliptic and inclined orbits of the asteroids, and different configurations for the positioning of observation spacecraft. It was found, that the resulting orbital elements were mostly independent of the positioning of the spaceborne observatories. The only noticeable effects were, that the days, where virtual measurements could not be performed due to occultation of the line of sight between spacecraft and asteroids by the Sun, dropped from 22 in 3652.5 days to approximately one, when either one of the spacecraft or the asteroid had an initial inclination, and that a dramatic decrease of the distance between the obervers worsened the results. The arguments for this behavior are very intuitive, as with initial inclination, the triangle $\mathbf{S}_1\mathbf{H}\mathbf{S}_2$ was no longer confined to the ecliptic, so the possibility for the Sun to intersect the line of sight decreased dramatically. Reducing the mutual distances of the spacecraft will result in the angles α and β* being around 90°, a configuration prone to produce large errors, as can be seen in section 3.4. A massive influence on the quality of the resulting orbital elements exerted a modification of eccentricities. Due to the fact, that the velocities of the asteroid **H** have to be interpolated with fixed order algorithms, a change in orbital velocities, e.g. near perihelion, will increase interpolation errors drastically, leading to comparatively large deviations from the true orbital elements. The importance of velocity interpolation also mirrors the fact that a reduction of time intervals between observations causes a decrease in orbital element errors, which was of the same order as the interpolation method used.

As an example, a probable asteroid - spacecraft configuration is examined more in detail, the initial orbital elements are to be seen in Table 2. The total simulation time was chosen to be 3652.5 days, consecutive observations were fixed to take place once a day. The two upper pictures in Figure 5 show the time development of deviations ΔH and Δv_H from the triangulated positions **H** and velocities v_H to the reference values taken directly from numerical integration results. The middle ones denote the corresponding development of measured angles α, β[6], θ_1 and θ_2. The maximum deviations ΔH are found at "unfavorable configurations" of $\mathbf{S}_1$, $\mathbf{S}_2$, **H** (see section 3.4) which are reached at $\alpha = \beta \simeq 0°$ *or* 180°. The largest Δv_H values at perihelion positions of the asteroid, where the rate of change of the asteroid's velocity vector will be higher, and therefore the interpolations' results deteriorate. Compared to the triangulation of the position vector of **H**, the errors due to velocity interpolations are larger by orders of magnitudes. As the positioning of **H** is, however, independent of the velocity error, all angular orbital elements are very well approximated. Of course, using more observations, one is able to apply higher order interpolation schemes, e.g. Stirling-interpolation, combining three consecutive positionings of the asteroid. This

[6] Please note that this is in fact the measured angle β not its calculated supplementary β*.

will reduce Δv_H curves' amplitudes in proportion to the order of the method applied. Adding a positioning uncertainty of 10^{-7} $[AU]$ [7] for each spacecraft, the lower left picture in Figure 5 unveils the consequent growth of error in ΔH to be in the order of magnitude of the positioning uncertainty itself, as was to be expected from equation (7). The effects on Δv_H as produced by Stirling-interpolation are detectable, as can be seen in the lower right picture, but they do not outweigh the influence of perihelion passages for high eccentricities. Using linear velocity interpolation, perturbations caused by positioning errors will not even register due to higher errors produced by the interpolation method itself.

Table 3 shows the quantitative behavior of the simulated triangulation of the position of **H**. In general, finite light travel time induced positioning errors of **H** had the largest influence on $\widetilde{\Delta H}$. This is partly due to the fact, that the linear approximation of the displacement is only valid for small light travel time differences, causing an unnatural displacement of **H** for larger separations. Still the errors produced by linear velocity interpolation dominate the effects induced by the optional error components (see Table 4). The data gained by Stirling velocity interpolation suffer proportionally more from additionally introduced errors.

table units $[AU]$	ΔH_{max}	ΔH_{min}	$\widetilde{\Delta H}$	$\widetilde{D}_{\Delta H}$
ideal	3.410E-12	4.728E-16	1.007E-14	6.927E-15
positioning error ($10^{-7}[AU]$)	5.242E-07	5.012E-09	1.494E-07	5.157E-08
angular measurement error ($0.126''$)	2.004E-02	9.592E-07	3.720E-06	2.045E-06
finite light travel time	6.193E-01	2.936E-09	1.157E-04	7.688E-05

Table 3 Statistical parameters for positioning of **H** via triangulation. ΔH signifies the deviation from the asteroid's original position to the triangulation result. Satellite positioning and angular measurement errors are given for each spacecraft and all angles.

table units $[\frac{AU}{D}]$	interpolation	$\Delta v_{H_{max}}$	$\Delta v_{H_{min}}$	$\widetilde{\Delta v_H}$	$\widetilde{D}_{\Delta v_H}$
ideal	linear	1.483E-04	1.641E-05	2.470E-05	7.957E-06
	Stirling	1.044E-06	1.281E-08	4.165E-08	2.815E-08
positioning error	linear	1.485E-04	1.598E-05	2.473E-05	7.976E-06
($10^{-7}[AU]$)	Stirling	1.127E-06	5.318E-09	1.739E-07	7.315E-08
angular measurement	linear	2.014E-02	2.406E-07	3.160E-05	1.491E-05
error ($0.126''$)	Stirling	1.005E-02	9.404E-09	2.722E-06	1.748E-06
finite light	linear	6.279E-01	1.864E-06	2.436E-05	1.120E-05
travel time	Stirling	3.118E-01	1.268E-07	2.686E-06	1.107E-06

Table 4 Statistical parameters for deviation of the asteroid's interpolated velocities from their reference values for different error scenarios. The timespan between consecutive observations was one day.

[7] 10^{-7} $[AU]$ is the approximate accuracy of DDOR Radar positioning.

5 Simulated Orbit Determination of Real Celestial Bodies

In order to be able to compare simulation results to real data on celestial bodies, a sample of four potentially hazardous asteroids (PHA) has been treated (Eggl, 2008). As all of them showed similar behavior concerning the simulated effects of the triangulation method, just one has been chosen to be presented here, namely **(2007 JY2)**. Initial orbital elements valid for the epoch J2000 as well as their corresponding standard deviations are shown in Table 5. The simulation has been performed as follows:

Initial conditions for the Solar System's main bodies, i.e. the Sun and the 8 planets, as well as for the observation spacecraft, arbitrarily positioned in the Lagrangian points L_4 and L_5 of the Sun-Earth system are being acquired for the epoch J2000. The Solar System, together with the observing spacecraft and one PHA are being propagated by numerical integration of the non-relativistic equations of motion using an order-controlled Lie-Series integrator (Eggl, Dvorak, 2010) for a total time of 3600 $[D]$. As the choice of the time-span between observations is crucial for the interpolation of a PHA's velocity, the following time-steps have been chosen: $\Delta t = 0.04\ [D] \simeq 1\ [h], 0.4\ [D], 4.0\ [D]$ and $40\ [D]$. The velocity interpolation is being done via linear interpolation, using two observations only, and Stirling-interpolation using three observations respectively. Having acquired data on positions and velocities at different times for all bodies involved, a series of virtual measurements of the required angles in $\mathbf{S}_1$: α, θ_1, in $\mathbf{S}_2$: β, θ_2 as well as the heliocentric position-vectors of the observing spacecraft $\mathbf{S}_1$ and $\mathbf{S}_2$ can be performed. Optional error components as introduced in section (4.1) were added during this process. In a next step the orbit determination is simulated as discussed in section (3.1). The results of the simulated measurements ($= \mathbf{OE}_{triangulation}$) are being compared to the quasi-flawless orbital elements directly calculated from the position and velocity output of the numerical integration ($= \mathbf{OE}_{integration}$). Finally the median values and median deviations of the differences of the simulated measurements to the flawless orbital elements are being plotted against the time-step, for linear-, and Stirling-interpolation of velocities.

The results can be studied in Figures 6 and 7. Ideal measurements, denoted by triangles, will result in fast and accurate orbital elements, where naturally Stirling-interpolation of velocities allows for better elements by using three consecutive observations. Interestingly, if observational errors are taken into account, the results for linear and second order interpolation algorithms become very similar. Even-though shorter observation intervals would serve ideal velocity interpolations, an optimum time-separation of $\simeq 0.4\ [D]$ is found, which is due to an error-proneness of velocity interpolation algorithms to miss-positioning of the asteroid given short time intervals. Another surprise may lie in the fact, that the Earth-spacecraft configuration (squares) - although punished by seeing - is seemingly able to compete with spacecraft-spacecraft configurations. This can be explained by the selected sample of observations performed by the Earth-spacecraft configuration due to the exclusion of all possible measurements that would have happened during daytime. Consequently only about 30% of all possible measurements remained, favoring those with the asteroid at aphelion position, where the changes in velocities are small and therefore the interpolation methods provide better results. All in all, comparing the simulation's outcomes to the accuracy of the orbital elements published by Solar System Dynamics Group, JPL (2010) (see Table 5), the triangulation method presented in this paper is more than competitive, for it provides orbital elements of comparable quality with two observations only.

a [AU]	e []	i [°]	ω[°]	Ω[°]	M[°]	mass[$M_\odot$]
2.19956074	0.68806235	1.5955816	105.080281	225.738210	329.8208272	0
σ_a [AU]	σ_e []	σ_i [°]	σ_ω[°]	σ_Ω[°]	σ_M[°]	
0.0031225	0.0005391	0.0016273	0.0037194	0.00049895	0.69888	

Table 5 Initial conditions (heliocentric orbital elements for epoch J2000) and standard deviations for the potentially hazardous asteroid (2007 JY2) published by the Solar System Dynamics Group, JPL (2010); these elements have been acquired from 78 observations spanning a data arc of 31 days.

6 Summary and Discussion

In this paper the possible refinement of asteroids' orbital elements via simultaneous observation from two spacecraft and consequent triangulation has been explored. After a brief description of the method proposed, an error propagation analysis uncovered some "unfavorable configurations" (UC) where triangulation is no more possible. A simulation of a full measurement process, including optional error components of fictitious asteroids, confirmed the existence of UC, and allowed for estimates on their influence and number of their occurrences (see Figure 5). It could be shown, that measurement errors have greater effects around UC (see Figure 2). Even-though, the dominant effects on the triangulated elements are caused by deviations of velocities due to interpolations' deficiencies (see Tables 3 and 4). Consequently, gaining the object's velocity by alternative methods, for example simultaneous high precision radar Doppler shift measurements would improve the outcome. The simulation was extended to real asteroids, where the results could be compared to current data provided by the Solar System Dynamics Group, JPL (2010), showing that the triangulation method was able to produce refined orbital elements of equal quality in a fraction of the time necessary for conventional methods. Taking observational inaccuracies into account, it was found that, although shorter observation intervals would favor ideal measurements, an optimum time-separation of $\simeq 0.4$ $[D]$ gives the best approximations to the asteroid's orbital elements a and e. The main limitation of the triangulation method proposed is the fact, that the approximate heliocentric position of the observed asteroid has to be known, in order to allow for a simultaneous observation from both spacecraft. Therefore it is not usable for initial orbit determination in its current formulation. Nevertheless there are numerous advantages, concerning refinement of orbital data on NEAs, such as the production of very accurate orbital elements with a minimum of necessary observations, re-usability, variability in positioning of the observing spacecraft and the fact that only few configurations prevent measurements. All in all, the method proposed would allow for a frequent and reliable update on NEAs' orbital elements, and could help keeping track of PHAs, which can undoubtedly be considered a very important topic, as one day our very lives may depend on it.

Acknowledgements The author would like to thank Rudolf Dvorak for his advice and the invitation to the 7th Humboldt Colloquium on Celestial Mechanics, Sylvio Ferraz-Mello and Jossaphat Gromaczkiewicz for very useful discussions, and last but not least Alessandra Celletti and Giovanni B. Valsecchi for their scientific hints in Bad Hofgastein. Additionally the author acknowledges the support of FWF project P-20216.

References

Chamberlin, A., Yeomans, D., Giorgini J., Chodas, P., Standish, M., Jacobson, R., Keesey, M., Ostro, S.: Solar System Dynamics Group, JPL/Caltec NASA `http://ssd.jpl.nasa.gov` (2010)

Eggl, S.: Effizienzstudie zur simultanen Berechnung der Bahnelemente von Near Earth Asteroids mit Hilfe zweier Satelliten. diploma thesis, University of Vienna Library, (2008)

Eggl, S., Dvorak, R.: An Introduction to Common Numerical Integration Codes Used in Dynamical Astronomy. Lecture Notes in Physics 790, *p. 431-477* (2010)

Gromaczkiewicz, J.: Trigonometric calculation of the elements of orbit of celestial bodies by two telescopes situated in the Lagrangian points L_4 and L_4. Proceedings of the 4th Austrian Hungarian workshop on celestial mechanics, Department of Astronomy of Eötvös University, *p. 21-33* (2006)

Gronchi, G.F., Dimare, L., Milani, A.: Orbit determination with the two-body integrals. Celestial Mechanics and Dynamical Astronomy 107, *p. 299-318* (2010)

Guthmann, A.: Einführung in die Himmelsmechanik und Ephemeridenrechnung. Spektrum Akademischer Verlag, 2. Auflage, *p. 195 ff* (2000)

Hanslmeier, A., Dvorak, R.: Numerical integration with Lie-series. Astronomy and Astrophysics 132, *p. 203-207* (1984)

Milani, A., Sansaturio, M.E., Chesley, S.R.: The asteroid identification problem IV: Attributions. Icarus 151, *p. 150-159* (2001)

Milani, A., Gronchi, G.F., de' Michieli Vitturi, M., Knežević, Z.: Orbit Determination with Very Short Arcs. I Admissible Regions. Celestial Mechanics and Dynamical Astronomy 90, *p. 57-85* (2004)

Milani, A., Gronchi, G.F.: Theory of Orbit Determination. Cambridge University Press, Cambridge (2009)

Morbidelli, A., Bottke, W.F.Jr., Froeschlé, Ch., Michel, P.: Origin and evolution of Near Earth Objects - Asteroids III. University of Arizona press, *p. 409-422* (2003)

Sachs, L.: Angewandte Statistik. Springer Verlag, *p. 337* (1999)

Tommei, G., Milani, A., Rossi, A.: Orbit determination of space debris: admissible regions. Celestial Mechanics and Dynamical Astronomy 97, *p.289-304* (2007)

Vesely, F.: Computational Physics - An Introduction. Springer US, (2001)

Wright, E. L. et al.: The Wide-field Infrared Survey Explorer (WISE): Mission Description and Initial On-orbit Performance. submitted to Astrophysical Journal, arXiv:1008.0031v1 [astro-ph.IM] (2010)

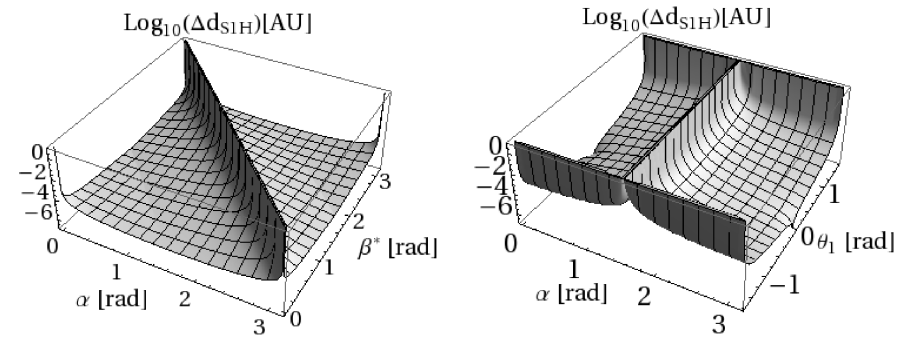

Fig. 2 Absolute error propagation for Δd_{S_1H}, containing measurement errors as pointed out in Table 1. *left:* vertical angle θ_1 is fixed at $\pi/4$, α and β* are varied, *right:* horizontal angle β* is fixed at $\pi/2$, α and θ_1 are varied.

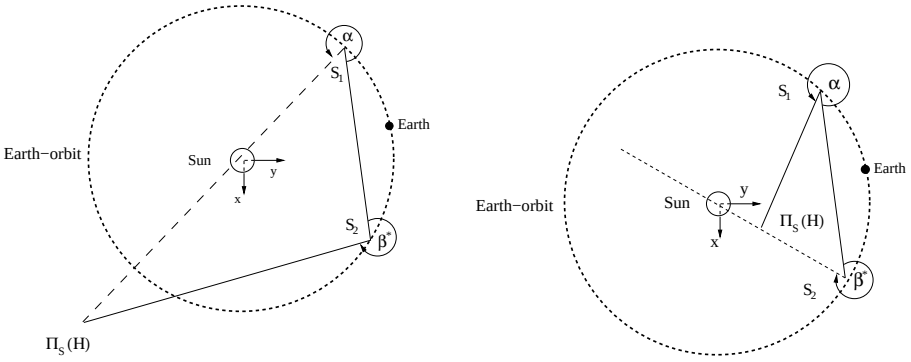

Fig. 3 Occultation of line of sight of one spacecraft by the Sun, orthogonal projection to the observers' reference plane, spacecraft are positioned in the ecliptic. $\mathbf{S}_1$ and $\mathbf{S}_2$ are spacecraft observatories, $\mathbf{H}$ the observed celestial body. $\Pi_S(\mathbf{H})$ denotes the orthogonal projection of $\mathbf{H}$ to the spacecraft's reference plane. *left*: The Sun blocks the line of sight of $\mathbf{S}_1$ concerning $\mathbf{H}$ *right*: If $\mathbf{H}$ moves in front of the Sun as seen from $\mathbf{S}_2$, an observation becomes impossible, due to the Sun's glare.

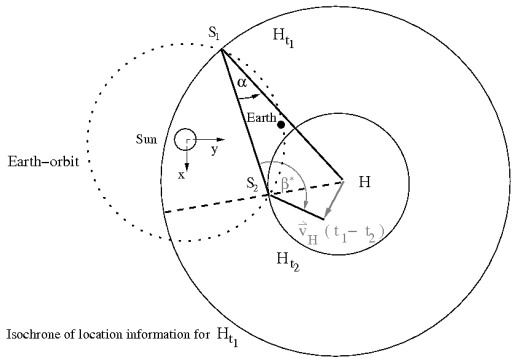

Fig. 4 The positioning error due to different light travel times of the location information of $\mathbf{H}$. This error depends on the distances $\|\mathbf{S}_1\mathbf{H}\|$, $\|\mathbf{S}_2\mathbf{H}\|$, as well as the velocity $\mathbf{v}_H$.

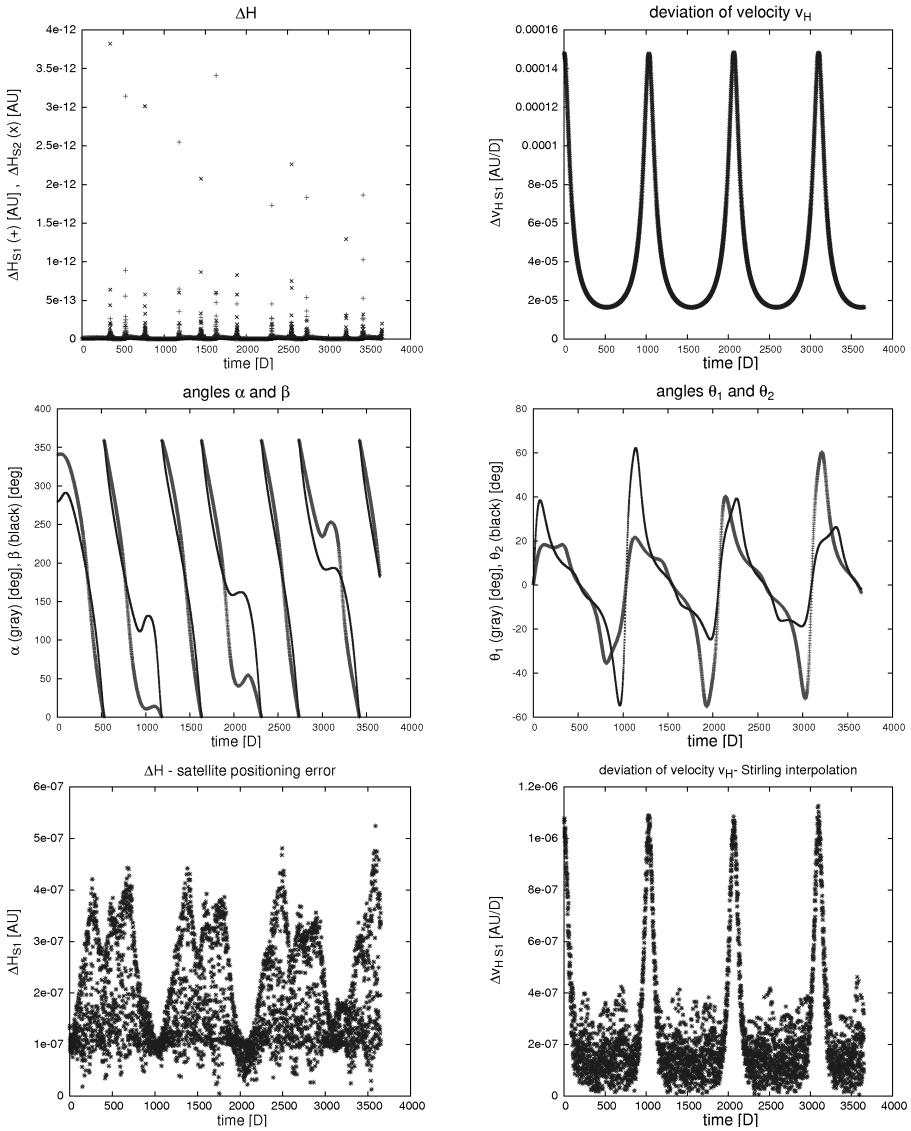

Fig. 5 Time development of the norms of deviations ΔH and Δv_H from the triangulated positions $\mathbf{H}$ and velocities $\mathbf{v_H}$ to the reference values taken directly from numerical integration results (see Table 2); *upper left*: ΔH from reference-positions for spacecraft $\mathbf{S}_1$ (+) and $\mathbf{S}_2$ (x) for ideal observations, *upper right*: corresponding Δv_H from reference-velocities for spacecraft $\mathbf{S}_1$ using linear interpolation, *mid left*: horizontal measurement angles α (gray) and β (black), *mid right*: vertical measurement angles θ_1 (gray) and θ_2 (black), *lower left*: ΔH for spacecraft $\mathbf{S}_1$ including positioning errors of $10^{-7}[AU]$ for each observer, *lower right*: corresponding Δv_H from reference-velocities for spacecraft $\mathbf{S}_1$ using Stirling-interpolation. The largest ΔH are found in the vicinity of "unfavorable configurations" (see section 3.4) which are reached at $\alpha = \beta \simeq 0°$ *or* 180°, the largest Δv_H values at perihelion positions of the asteroid. Stirling velocity interpolation yields better approximations for the velocities, but is more susceptible to measurement and spacecraft positioning errors. Time between consecutive observations was fixed to 1 $[D]$.

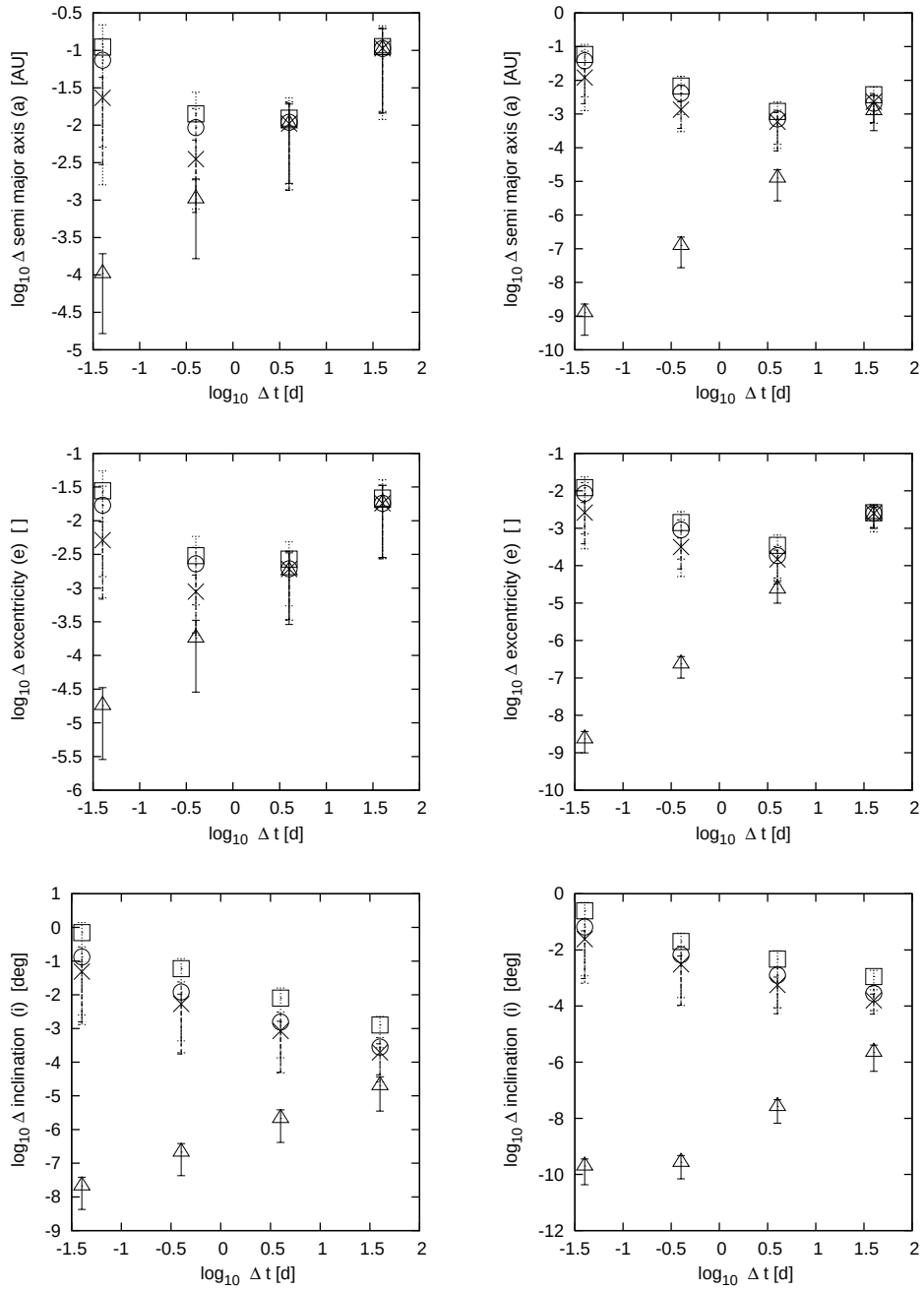

Fig. 6 median and median deviations (errorbars) of the difference between original and measured orbital elements (a,e,i) of **(2007 JY2)** over 3600 [D]
left column: two consecutive observations separated by Δ t days used
right column: three consecutive observations separated by Δ t days used
non-ideal observations contain all error sources discussed in section 4.1
triangle: ideal observation from two spacecraft in L_4 and L_5 of the Sun-Earth system
cross: non-ideal observation from two spacecraft (L_4, L_5, diffraction limited, diameter 1 [m])
circle: non-ideal observation from two spacecraft (L_4, L_5, diffraction limited, diameter 0.3 [m])
square: non-ideal observation in spacecraft (L_4) - Earth configuration
(diffraction limited, diameter 1 [m] + seeing 2 ["])

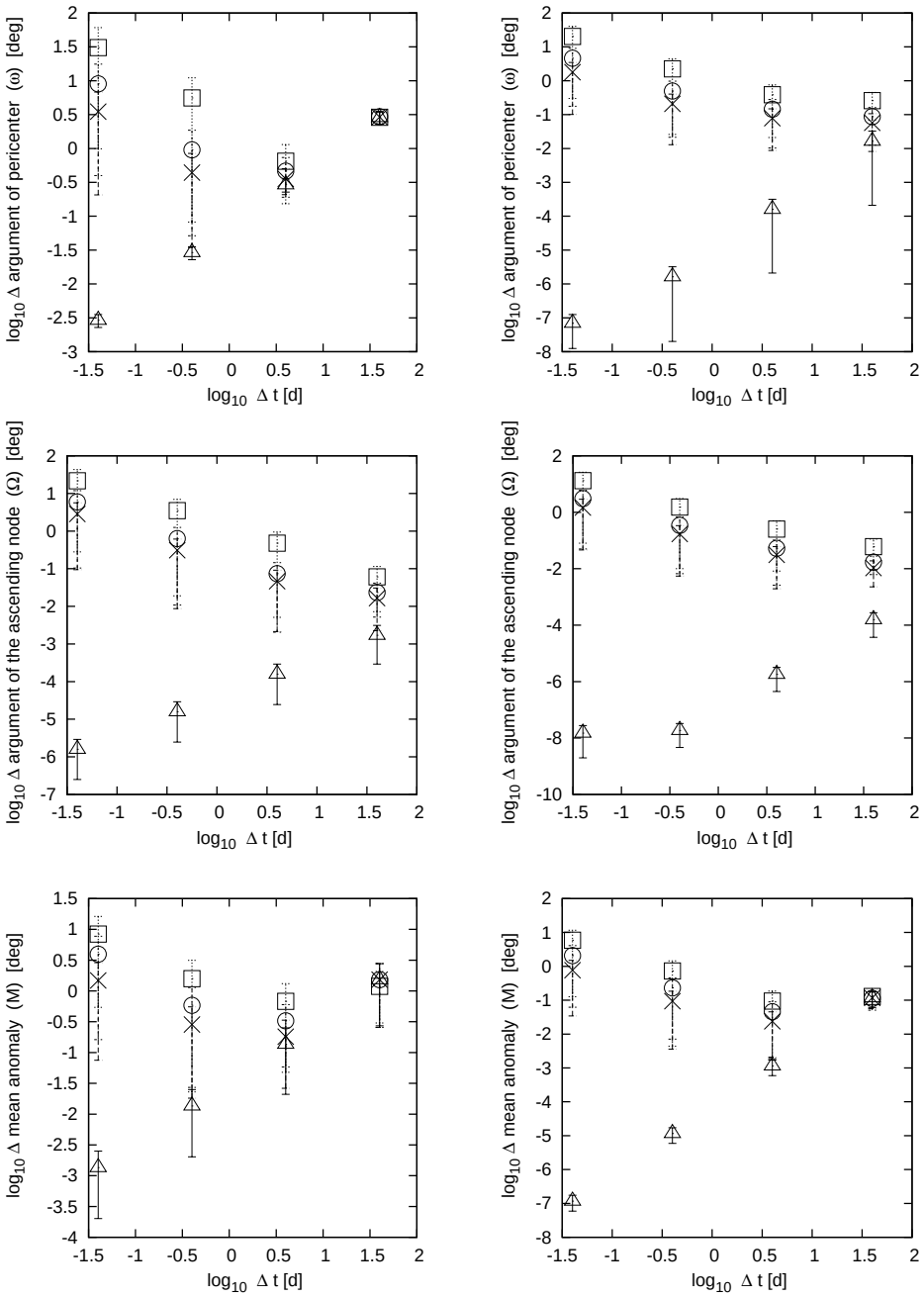

Fig. 7 median and median deviations (errorbars) of the difference between original and measured orbital elements (ω, Ω, M) of **(2007 JY2)** over 3600 $[D]$
left column: two consecutive observations separated by Δ t days used
right column: three consecutive observations separated by Δ t days used
non-ideal observations contain all error sources discussed in section 4.1
triangle: ideal observation from two spacecraft in L_4 and L_5 of the Sun-Earth system
cross: non-ideal observation from two spacecraft (L_4, L_5, diffraction limited, diameter 1 $[m]$)
circle: non-ideal observation from two spacecraft (L_4, L_5, diffraction limited, diameter 0.3 $[m]$)
square: non-ideal observation in spacecraft (L_4) - Earth configuration
(diffraction limited, diameter 1 $[m]$ + seeing 2 ["])